HHS Public Access

Author manuscript

*ACS Chem Biol*. Author manuscript; available in PMC 2017 February 19.

Published in final edited form as:

*ACS Chem Biol*. 2016 February 19; 11(2): 500–507. doi:10.1021/acschembio.5b00844.

# Human telomere G-quadruplexes with five repeats accommodate 8-oxo-7,8-dihydroguanine by looping out the DNA damage

**Na An**, **Aaron M. Fleming**, and **Cynthia J. Burrows***

Department of Chemistry, University of Utah, 315 S 1400 East, Salt Lake City, UT 84112-0850

## Abstract

Inflammation and oxidative stress generate free radicals that oxidize guanine (G) in DNA to 8-oxo-7,8-dihydroguanine (OG), and this reaction is prominent in the G-rich telomere sequence. In telomeres, OG is not efficiently removed by repair pathways allowing its concentration to build, surprisingly without any immediate negative consequences to stability. Herein, OG was synthesized in five repeats of the human-telomere sequence $(TTAGGG)_n$, at the 5′-G of the 5′-most, middle, and 3′-most G tracks, representing hotspots for oxidation. These synthetic oligomers were folded in relevant amounts of $K^+/Na^+$ to adopt hybrid G-quadruplex folds. The structural impact of OG was assayed by circular dichroism, thermal melting, $^1$H-NMR, and single-molecule profiling by the α-hemolysin nanopore. On the basis of these results, OG was well accommodated in the five-repeat sequences by looping out the damaged G track to allow the other four tracks to adopt a hybrid G-quadruplex. These results run counter to previous studies with OG in four-repeat telomere sequences that found OG to be highly destabilizing and causing significant reorientation of the fold. When taking a wider view of the human telomere sequence and considering additional repeats, we found OG to cause minimal impact on the structure. The plasticity of this repeat sequence addresses how OG concentrations can increase in telomeres without immediate telomere instability or attrition.

## Graphical Abstract

*To whom correspondence should be addressed: (801) 585-7290, burrows@chem.utah.edu.

Supporting Information

Detailed methods, current vs. time traces, current blocking histograms, expanded $^1$H-NMR spectra, and results of CD and $T_m$ in high salt conditions. This material is available free of charge via the Internet at http://pubs.acs.org.

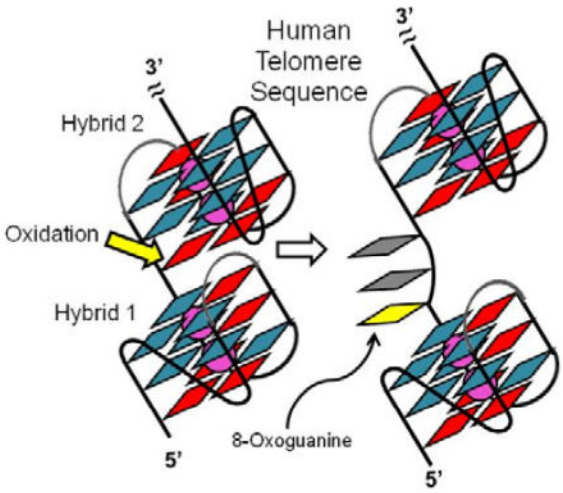


## Introduction

Stress to human cells can result from micronutrient imbalance, toxins, temperature extremes, mechanical damage, oxidative stress, or inflammation.[1] Molecular level details of how stressors impact cells are essential for understanding its consequences and developing treatments to combat the damage. More specifically, oxidative or inflammatory stress can generate free radicals capable of oxidizing biomolecules, of which the genome is a particularly deleterious target for oxidations.[2,3] DNA damage to most of the genome, if left unrepaired, can cause mutations leading to disease or cell apoptosis. Oxidation of guanine (G) to 8-oxo-7,8-dihydroguanine (OG) is a major reaction observed in free radical stress.[4] Generally in the genome, OG is efficiently cleared by the base excision repair (BER) pathway.[5,6] In contrast, telomeres have been found to accumulate OG without catastrophic impact on short-term cellular viability.[7–9] This observation lends to questioning how telomeres continue to function in the presence of increasing concentrations of OG.

Telomeres cap chromosome ends with kilobase-long runs of the repeating sequence 5′-$(TTAGGG)_n$-3′ in humans. Most of the telomere resides as a duplex with the exception of the 3′-terminal 50-200 nucleotides that are single stranded.[10] The G-rich nature of this sequence renders it highly susceptible to G oxidation to OG and other heterocycles, especially in the single-stranded region, because it is more exposed to react with diffusible oxidants.[11,12] Further, the repeating nature of the single-stranded region on the 3′ end allow formation of G-quadruplex (G4) structures.[13,14] Cellular demonstration of G4 folds in telomeres was achieved by immunofluorescence.[15] The presence of OG in duplex DNA represents an excellent context for its removal by the BER process. [5,6] On the other hand, when OG is present in single-stranded or G4 contexts, it is poorly repaired by the same pathways,[16,17] and alternative routes for removal of OG from these regions have not been identified. The lack of OG repair establishes a possible mechanism to address why OG remains in telomeres; however, details concerning the structural impact OG has on human telomere G4s have not been adequately addressed.

The single-stranded human telomere sequence adopts hybrid-1 or hybrid-2 G4 folds in potassium ion solutions (Figure 1A),[18–20] the relevant intracellular cation. Additionally, the human telomere sequence is highly dynamic in KCl solutions leading to significant populations of triplex folding intermediates.[21–23] We and others have conducted model studies with OG in the human telomere sequence in similar KCl solutions.[16,24–26] These experiments utilized a four-repeat section of this sequence, as it represents the minimum length to adopt a G4 fold. The main conclusion from these studies was that placement of OG in an exterior tetrad induces a structural reorientation based on circular dichroism (CD) analysis with a ~15 °C loss in the thermal stability ($T_m$). On the basis of the CD signatures, these OG-containing G4 strands have an antiparallel strand orientation, with possible partial G4 unfolding to a triplex species.[27] When OG was placed at the central tetrad, significant rearrangement of the structure occurs with nearly a 25 °C reduction in the $T_m$. We proposed when OG is in the middle tetrad the structure adopts an unstable triplex-like topology.[16] The inability of OG to form Hoogsteen base pairs with G drives these structural changes (Figure 1B), whereas oxidation at loop nucleotides has minimal impact on the structure.[28,29] From these studies, one would conclude that OG causes significant perturbation of the structures at the ends of telomeres; and it is quite surprising that OG can accumulate in this region of the genome without dramatically impacting chromosome stability.

In the present report, we took an expanded view and asked how OG impacts G4 folding with five repeats of the human telomere sequence, more than is strictly necessary for a G4 fold in the absence of guanine damage. Because the single-stranded overhang of the telomere typically has 8–35 repeats, the structural impact of OG would be better understood in this expanded view with five repeats. In these studies, OG was synthetically incorporated in place of the 5′ G in the 5′-most, middle, or 3′-most G runs (Table 1). The sites studied with OG have been demonstrated as highly reactive to yield OG with $CO_3^{\bullet-}$ oxidation, a major cellular oxidant found in inflammation.[11] Traditional structural methods (CD, $T_m$, and NMR) found OG to be well accommodated when the 5$^{th}$ repeat was considered in the analysis. Next, an innovative method utilizing the α-hemolysin (α-HL) nanopore was harnessed to profile the distribution of different folding topologies in solution.[30–33] From these studies, we conclude the repeat track containing OG was looped out to allow the other four repeats to establish hybrid-like G4 folds with minimal impact on the stability. Lastly, the distribution of the two different hybrids was altered depending on the run in which OG was placed. By taking a wider view of the human telomere sequence, we found OG to cause looping out of the damaged repeat while maintaining the overall architecture of the fold. Further, this provides a better molecular picture to explain how OG can be accumulated in the telomere without causing significant chromosomal instability.

## Results and Discussion

Site specific incorporation of OG in the hTelo sequences was achieved by solid-phase oligomer synthesis. The sequences were the natural form by having two nucleotide tails on the 5′ and 3′ ends (Table 1). The purified strands were initially studied utilizing CD and $T_m$ in relevant salt concentrations (140 mM KCl and 12 mM NaCl, buffered at pH 7.4), or by $^1$H-NMR (70 mM KCl, buffered at pH 7.0). The CD analysis identified the native strand hTelo5 to adopt a hybrid fold, on the basis of the $\lambda_{max}$ at 265 and 290 nm, and a $\lambda_{min}$ at 240

nm when compared to literature sources (Figure 2A).[34] When the five-repeat strands containing OG were studied, they all produced CD profiles nearly identical to the native sequence (Figure 2A). Specifically, they all had the same $\lambda_{min}$ and $\lambda_{max}$ values with slightly different intensities. Additionally, these spectra support hybrid folds for all sequences; however, the distribution of hybrid-1, hybrid-2, and triplex folds cannot be determined from these results. In contrast to the present five-repeat hTelo sequences studied, when OG was incorporated in four-repeat hTelo sequences, significant changes in the CD spectra were observed.[16,24–26] This initial observation supports a hypothesis that the OG-containing five-repeat G4s adopt structures that retain features of the wild-type sequence, a result that is nearly opposite to that previously reported in the literature for OG in four-repeat hTelo G4s.

To further probe the structures, imino $^1$H-NMR signals for the five-repeat hTelo G4s were recorded (Figures 2B and S1). The imino spectrum for the hTelo5 sequence yielded signals in the 10 – 12 ppm range diagnostic of G:G Hoogsteen base pairs when compared to literature values.[18–20] Further, this spectrum provided 20 identifiable peaks, an observation consistent with more than one G4 fold in solution, because one G4 fold would yield a maximum of 12 resolvable peaks. The imino spectrum for hTelo 5′-OG also produced 18 signals diagnostic of G:G Hoogsteen base pairs, supporting a mixture of folds in solution. When OG was placed in the middle run (hTelo OG-mid), the imino spectrum yielded signals indicative of G4 folding. Further, the spectrum had 19 identifiable peaks indicating a mixture of folds in solution. In the last NMR experiment, the hTelo 3′-OG sequence also yielded 19 imino peaks consistent with more than one G4 fold in solution. These NMR results add additional support for expanded hTelo sequences adopting G4 topologies with and without OG present.

In the next study, $T_m$ analysis was conducted on each G4 sequence. The $T_m$ value obtained for hTelo5 was 56.2 °C and the OG-containing sequences hTelo 5′-OG and hTelo 3′-OG had values nearly identical to the native sequence (55.6 °C; Figure 2C). When OG was synthesized in the middle run (hTelo mid-OG), the $T_m$ was ~5 °C lower than the native sequence hTelo5. These $T_m$ results identify OG to have no impact when found in a 5′ or 3′ tail, while the case with OG in the middle run caused the structure to have a small, but noticeably lower $T_m$ than the wild-type sequence (Figure 2C). This observation is in contrast to studies on the four-repeat hTelo sequence, in which OG dramatically decreases the $T_m$ (>15 °C).[16,24–26] Additionally, the $T_m$ values are slightly lower than wild-type, four-repeat hTelo sequences (~5 °C) reported in the literature, an observation that has previously been ascribed to long tails or loops decreasing the stability of G4 folds;[35] in these studies, the long tail or loop is the repeat not involved in G4 formation. The $T_m$ experiments further support the conclusion that five-repeat hTelo sequences can accommodate OG without significant impact on G4 stability.

The findings from CD, $^1$H-NMR, and $T_m$ analysis found OG to be well accommodated in the hTelo sequence when five hexanucleotide repeats were considered. The CD spectra for hTelo with OG were nearly identical to the wild-type sequence, and the $T_m$ values for the wild-type and OG-containing hTelo sequences were all nearly the same, with the exception of OG in the middle run. Moreover, the $^1$H-NMR spectra support G4 formation for all sequences studied, and the results support a mixture of folds. Nevertheless, these

experiments leave a few lingering questions: What are the folds and their distribution for the five-repeat hTelo sequence? Does the presence of OG at the 5′ run, middle run, or 3′ run alter the folds and their distributions? On the basis of previous studies from our laboratory,[30–32,36] one approach to address these questions is to profile the topologies in solution with the α-HL nanopore. In this experiment, a single, small aperture protein nanopore is embedded in a lipid bilayer and an electrophoretic force is applied to drive a single, DNA molecule into the nanocavity (Figure 3).[37–39] The opening to the nanocavity is of appropriate dimensions to allow entry of the hybrid and triplex folds observed in KCl solutions. Once they enter the nanocavity, fluctuations to the ion current are recorded giving diagnostic signatures for hybrid-1, hybrid-2, and triplex folding intermediates while they are trapped before exiting the channel. They can exit either by unraveling and traveling to the *trans* side of the pore, or diffusion can cause the folded DNA to exit back out the *cis* side of the channel from which they entered. Therefore, we applied the nanopore system to interrogate the folds and their distributions for the five-repeat hTelo sequences in the present study. In order to obtain enough events at reasonable DNA concentrations (5 μM), the ionic strength was held at 1 M. In these studies, we used 50 mM KCl mixed with 950 mM LiCl to obtain the desired ionic strength. The CD and $T_m$ experiments were repeated under these high salt conditions and compared to the studies described above (Figures 2A and 2B) and provided similar results for the two different salt systems (Figure S2).

In the nanopore experiments, the DNA was placed on the *cis* side of the channel and a 120 mV bias (*trans* vs. *cis*) was applied to electrophoretically pull the G4 folds into the nanocavity of α-HL. We observed current vs. time (*i-t*) patterns with the five-repeat G4s that were identical to four-repeat G4s from our earlier studies.[30] The ion currents are reported as the percentage of blocking current recorded when DNA interacts with the channel divided by the open channel current when the pore is void of DNA (i.e., $\%I/I_o$). As an additional note, the rate at which different folds enter the nanocavity of α-HL are not the same, and correction factors for these differing event frequencies were previously determined, and applied to the present results (hybrid-1 : hybrid-2 : triplex = 1.0 : 0.9 : 6.2).[30] Analysis of >500 interactions between the G4s and α-HL from three unique experiments provided two populations of blocking-current event types (Table 2). The Type 1 events represented 21 ± 2% of the total population and produced a blocking residual current of $\%I_1/I_o$ = 8 ± 2% (Figures 3 and S3). A histogram of the event time durations was exponentially distributed with a time constant of 0.8 ± 0.1 ms (Figure S4). On the basis of a comparison to our previous results,[30] we propose these event types represent the triplex-folding intermediates, and their presence is consistent with other experimental and theoretical studies.[21–23] The triplex folds were able to unravel under the applied electrophoretic force and pass through the β-barrel and exit the *trans* side of the channel. Support for this claim was achieved by a voltage-dependent study while monitoring the event duration time. In this study, as the voltage was increased the event time decreased, supporting translocation of the triplex folds, because as the force increases the unraveling process occurs more quickly (Figure S4).

The second event population termed Type 2 represents the characteristic ion-current patterns for hybrid-1 and hybrid-2 G4s. The Type 2 events represented 72 ± 8% of the total events (Table 2). The *i-t* traces initiated from $I_o$ to a midlevel blockage of either $\%I_{m1}/I_o$ = 37 ± 2% for hybrid-1 or $\%I_{m2}/I_o$ = 44 ± 2% for hybrid-2 (Figure 3). These intermediate levels

oscillated to a deep blockage of $\%I_D/I_o = 10 \pm 2\%$ for both hybrid-1 and hybrid-2 folds. In four-repeat hTelo G4s these midlevel blockage currents were diagnostic of the hybrid folds.[30,32] Using these diagnostic currents allowed counting the number of events that adopt hybrid-1 and hybrid-2. The ratio of hybrid-1 to hybrid-2 was found to be 1.6:1.0 (Table 2), a value that differs from four-repeat hTelo sequences that have a hybrid-1 to hybrid-2 ratio of 2.3:1.0.[30] Other experimental studies show strong preference for hybrid-1 over hybrid-2 in the four-repeat hTelo sequence.[19,20,41,42] This comparison identifies addition of the fifth repeat to shift the hybrid ratio away from hybrid-1; though, hybrid-1 still represents the major fold in solution.

Analysis of the duration times for the Type 2 events found two distributions, one lasted 10–100 ms, while the second population progressed for >10 s (Figure 4). As a note, regardless of the time distribution, the oscillation between the deep current level around 10% and a midlevel currents at either 37% for hybrid-1 or 44% for hybrid-2 were observed. We propose these two time distributions result from the entry orientation of the folds. In the events that lasted 10–100 ms, the G4 cap entered first with the tail protruding from the *cis* opening of the channel (Figure 4). These events progressed until the G4 diffused back out of the channel via the *cis* opening. For the events that lasted >10 s, they entered via the 8-mer tail not involved in G4 formation. The tail entered the β-barrel to provide a handle for the electrophoretic force to trap the G4 for longer times (Figure 4). The increase in trapping time is consistent with our previous studies, in which a 25-mer homopolymer tail was appended to the hybrid G4s allowing trapping in the α-HL channel for up to 4 min.[31] Interactions that produced the Type 2 events all terminated by diffusion of the G4 back out the *cis* side of the channel. This claim is supported by a voltage-dependent study that established as the voltage was increased the event time increased, due to the increase in electrophoretic force decreasing the rate of DNA diffusion out of the channel (Figure S5). There existed $<7 \pm 1$ % of the events that did not fit into the triplex, hybrid-1, or hybrid-2 categories, and their identification was not pursued (Figure S3). These results with hTelo5 provide the patterns used to identify how OG introduced at each site impacts the distribution of hybrid-1, hybrid-2, and triplex folds.

Introduction of OG into the five-repeat sequence produced positional dependency in the folding distributions. The folding distribution observed with hTelo 5′-OG was 24% triplex, 33% hybrid-1, and 36% hybrid-2, and the hybrid-1 to hybrid-2 ratio was 0.9:1.0 (Table 2). When OG was placed in the 5′-repeat track causing this repeat to remain single stranded, the ratio of hybrid-1 compared to hybrid-2 was nearly the same, an observation in contrast to the native sequence that favored hybrid-1 by nearly twofold. Evaluation of hTelo 3′-OG produced a mixture composed of triplex, hybrid-1, and hybrid-2 in 18%, 45%, and 29%, respectively (Table 2). For the hTelo 3′-OG, the tail must be on the 3′ side to produce a hybrid-1, hybrid-2 ratio of 1.5:1.0, a value similar to the native sequence hTelo5 (1.6:1.0). Studies for hTelo mid-OG failed to produce *i-t* signatures for hybrid-1 and hybrid-2, and the only events observed were the triplex-folding intermediate (Table 2). The CD, $^1$H-NMR, and $T_m$ results support hybrid G4 formation for hTelo mid-OG (Figure 2), and the inability to observe these signatures in the α-HL nanopore experiment must result from loop formation in the middle of the G4 causing the structure to be too large to enter the nanocavity. This observation points to one limitation of the α-HL nanopore, in which structures that are too

large to pass the mouth of the nanocavity cannot be studied by this method.[43] In spite of this limitation, the nanopore results identified hybrid G4s when OG was synthesized site specifically in the hTelo 5′-OG and hTelo 3′-OG sequences. Similar to the hTelo5 sequence, the OG-containing hTelo sequences yielded events ~7% of the time that were not assigned to a structure.

There exists a dependency of the hybrid ratio with respect to the 5′ vs. 3′ tail side; for example, the native sequence and hTelo 3′-OG adopt similar hybrid-1 to hybrid-2 ratios (~1.6:1.0), both favoring hybrid-1 (Table 2). In contrast, hTelo 5′-OG provided a significant increase in hybrid-2. Interpretation of these results supports hybrid folds showing a preference for the tail to be furthest from the double-chain reversal loop that defines hybrid-1 or hybrid-2. In hTelo 5′-OG with a 5′ tail, the amount of hybrid-2 with a 3′ double-chain reversal loop significantly increased, while hTelo 3′-OG with a 3′ tail favored hybrid-1, with the double-chain reversal loop on the 5′ side (Figure 1 and Table 2). Interestingly, hTelo5 gave a similar hybrid ratio as hTelo 3′-OG, supporting the conclusion that the native sequence with five repeats of the telomere sequence possibly favors the tail on the 3′ side. Unfortunately, hTelo mid-OG could not be studied with respect to hybrid ratios. Additionally, looping out a damaged G-track into an edgewise loop as occurred in hTelo mid-OG is an unlikely scenario in the context of a full-length telomere. A full length telomere will have >8 repeat sequences in the single-stranded 3′ overhang, and hTelo mid-OG had the lowest $T_m$ by ~5 °C suggesting that a long, edgewise loop is less stable than the tail on the 5′ or 3′ side, as observed for hTelo 5′-OG and hTelo 3′-OG (Figure 2C). Therefore, in the event of G oxidation to OG in full length telomeres, the damaged loop will migrate to the 5′ or 3′ end of the G4 structure to maintain folds with three-nucleotide loops (Figure 5).

## Conclusions

The peripheral location of telomeres on chromosomes, their richness in G nucleotides, and their single-stranded termini cause them to be hotspots for free radical damage resulting from oxidative and inflammatory stress. Oxidation of G to OG is a major reaction channel in cells supported by findings that OG concentrations are greater in telomeres than the interior of the chromosome.[7–9] Additionally, for OG concentrations to increase, OG must evade the repair process as evident by the inability of OGG1 to operate on single-stranded or G4 contexts;[16,44] moreover, the presence of OG in the telomere does not lead to catastrophic chromosome instability.[7–9] When OG was studied in four repeats of the human telomere sequence, significant distortion of the structure and great loss in thermal stability was observed,[16,24–26] an observation in stark contrast to the conclusions drawn from the cellular studies. The present work took a wider view and studied the impact of OG on five repeats of the human telomere sequence, and found OG to be silent with respect to thermal stability and impact on the greater structure when compared to the undamaged sequence (Figures 2 and 3). These findings add much needed clarity to understand how OG can persist in telomeres without causing detrimental impact on its structure.

Taking a larger view of how the single-stranded region of the telomere folds provided additional details about the telomere structure as well as how it responds to oxidative insults.

Studies on four-repeat hTelo G4s find a strong preference for hybrid-1 over hybrid-2 folds;[19,20,30,41,42] in contrast, when a larger number of repeats were studied, as we did here, the strong hybrid-1 preference diminishes (Table 2). Chaires and Trent proposed strings of hybrid G4s would alternate between hybrid-1 and-2 to allow stacking.[45] These studies provide additional insight into this model for natural telomeres that have the duplex region attached to the 5′ end; thus, the first hybrid fold could be hybrid-2 favoring the double-chain reversal loop furthest from the duplex, and the next would by hybrid-1 (Figure 5). In the event of G oxidation yielding OG, the structure could roll looping out the damaged repeat sequence. Because placement of the damaged repeat in an edgewise loop caused the greatest decrease in $T_m$ (Table 2C), the telomere structure would roll to place the damaged repeat in a single-stranded region between two hybrid G4s (Figure 5). Having a single-stranded region in long telomeres might be a natural occurrence on the basis of previous studies by Petraccone, et al., who studied telomere sequences in solution that could fold up to three contiguous G4s.[46] In their studies, the sequence adopts the maximum number of G4s ~90% of the time and ~10% adopted two G4s with single-stranded regions. Additionally, when long, human-telomere sequences were studied on surfaces or by optical tweezers incomplete folding was observed for the sequences also showing single-stranded regions.[47–49] The percentage of single-stranded regions is anticipated to increase as the number of possible G4s increases. Telomere sequences bearing OG are substrates for G4-unwinding helicases (i.e., WRN and BLM) and these sequences are bound more tightly by POT1, the telomere specific single-stranded binding protein, than the native sequence.[50] Thus, OG will hide in an already expected single-stranded region of these polymorphic sequences, and OG has minimal impact on the activity of proteins that interact with the telomere, explaining how it can persist in these regions.

Oxidation of G to OG in the human telomere induces a reorientation of the structure that must mask the damage to avoid significant instability of the telomere leading to cell death. This feature was recently identified by our laboratory to also exist in a large number of G4 sequences found in gene promoters, in which a fifth-G run appears in tandem with the core-G runs.[51] We ascribed the fifth-G run the role of a “spare tire” to maintain G4 folding in the event of G oxidation. A number of studies are finding important functions for G4s in cells,[52] and the G-rich nature of these sequences render them hotspots for oxidation. Therefore, preservation of G4 folding in the event of oxidation appears to be solved by biology via selection of sequences that have an additional G track in close proximity of the core. A conundrum with respect to OG is the fact that it is more prone to further oxidation than G yielding hydantoin products.[11] Interestingly, these products are good substrates for the NEIL glycosylases in the G4 context, particularly when a 5$^{th}$ G track is present.[51] For telomeres, high concentrations of OG will lead to high concentrations of hydantoins over time. Initiation of hydantoin repair in telomeric G4s will lead to telomere attrition with negative, long-term consequences to cellular survival. Thus, OG might not have devastating consequences initially, but its hyperoxidation product will have a dramatic impact.

## Methods

The oligonucleotides were synthesized by the DNA-Peptide Core Facility at the University of Utah, processed by standard protocols, and purified by ion-exchange HPLC as previously

described.[30] The CD and $T_m$ experiments were performed in salt solutions composed of either 12 mM NaCl, 140 mM KCl, with 20 mM cacodylate buffer (pH 7.4), or in 50 mM KCl, 950 mM LiCl, with 25 mM Tris (pH 7.9). The $^1$H-NMR spectra were recorded in 20 mM $KP_i$ (pH 7.0) with 70 mM KCl in 1:9 $D_2O$:$H_2O$ on an 800-MHz NMR spectrometer on 300 μM samples at 24 °C. Solvent suppression in the NMR experiments was achieved with a watergate pulse sequence.

The customized, low-noise amplifier and data acquisition system was provided by Electronic Biosciences for conducting the ion channel recordings. All electrolyte solutions were prepared with > 18 MΩ/cm ultrapure water that was filtered with a 0.22-mm Millipore vacuum filter. The wild-type α-HL nanopore was embedded in a lipid bilayer supported by a glass nanopore membrane that was constructed following literature protocols.[53] The data were recorded with a 100-KHz low-pass filter and a 500-kHz acquisition rate. The *i-t* traces shown in the manuscript were refiltered to 20 kHz for presentation purposes. QuB 1.5.0.31 and Igor Pro-6.1 were used to extract, analyze, and plot the events. The measurements were conducted at 22 °C.

## Supplementary Material

Refer to Web version on PubMed Central for supplementary material.

## Acknowledgments

This work was funded by grants provided by the National Institutes of Health (R01 CA090689, and in part, R01 GM093099). The authors appreciate colleagues at Electronic BioSciences (San Diego, CA) for supplying the instrument and software utilized for recording the current vs. time traces, and Profs. Henry White and Peter Flynn (University of Utah) for helpful discussions. The oligonucleotides were provided by the DNA/Peptide core facility at the University of Utah that is supported in part by the NCI Cancer Support Grant (P30 CA042014).

## References

1. Simmons SO, Fan CY, Ramabhadran R. Cellular stress response pathway system as a sentinel ensemble in toxicological screening. Toxicol Sci. 2009; 111:202–225. [PubMed: 19567883]
2. Delaney S, Jarem DA, Volle CB, Yennie CJ. Chemical and biological consequences of oxidatively damaged guanine in DNA. Free Radical Res. 2012; 46:420–441. [PubMed: 22239655]
3. Cadet J, Douki T, Ravanat JL. Oxidatively generated damage to cellular DNA by UVB and UVA radiation. Photochem Photobiol. 2015; 91:140–155. [PubMed: 25327445]
4. Gedik CM, Collins A. Establishing the background level of base oxidation in human lymphocyte DNA: results of an interlaboratory validation study. FASEB J. 2005; 19:82–84. [PubMed: 15533950]
5. David SS, O'Shea VL, Kundu S. Base-excision repair of oxidative DNA damage. Nature. 2007; 447:941–950. [PubMed: 17581577]
6. Wallace SS. Base excision repair: A critical player in many games. DNA Repair. 2014; 19:14–26. [PubMed: 24780558]
7. O'Callaghan N, Baack N, Sharif R, Fenech M. A qPCR-based assay to quantify oxidized guanine and other FPG-sensitive base lesions within telomeric DNA. BioTechniques. 2011; 51:403–410. [PubMed: 22150331]
8. Rhee DB, Ghosh A, Lu J, Bohr VA, Liu Y. Factors that influence telomeric oxidative base damage and repair by DNA glycosylase OGG1. DNA Repair (Amst). 2011; 10:34–44. [PubMed: 20951653]

9. Coluzzi E, Colamartino M, Cozzi R, Leone S, Meneghini C, O'Callaghan N, Sgura A. Oxidative stress induces persistent telomeric DNA damage responsible for nuclear morphology change in mammalian cells. PLoS ONE. 2014; 9:e110963. [PubMed: 25354277]
10. Verdun RE, Karlseder J. Replication and protection of telomeres. Nature. 2007; 447:924–931. [PubMed: 17581575]
11. Fleming AM, Burrows CJ. G-Quadruplex folds of the human telomere sequence alter the site reactivity and reaction pathway of guanine oxidation compared to duplex DNA. Chem Res Toxicol. 2013; 26:593–607. [PubMed: 23438298]
12. Alshykhly OR, Fleming AM, Burrows CJ. 5-Carboxamido-5-formamido-2-iminohydantoin, in addition to 8-oxo-7,8-dihydroguanine, Is the major product of the iron-Fenton or X-ray radiation-induced oxidation of guanine under aerobic reducing conditions in nucleoside and DNA contexts. J Org Chem. 2015; 80:6996–7007. [PubMed: 26092110]
13. Sen D, Gilbert W. Formation of parallel four-stranded complexes by guanine-rich motifs in DNA and its implications for meiosis. Nature. 1988; 334:364–366. [PubMed: 3393228]
14. Sundquist WI, Klug A. Telomeric DNA dimerizes by formation of guanine tetrads between hairpin loops. Nature. 1989; 342:825–829. [PubMed: 2601741]
15. Biffi G, Tannahill D, McCafferty J, Balasubramanian S. Quantitative visualization of DNA G-quadruplex structures in human cells. Nat Chem. 2013; 5:182–186. [PubMed: 23422559]
16. Zhou J, Fleming AM, Averill AM, Burrows CJ, Wallace SS. The NEIL glycosylases remove oxidized guanine lesions from telomeric and promoter quadruplex DNA structures. Nucleic Acids Res. 2015; 43:4039–4054. [PubMed: 25813041]
17. Jia P, Her C, Chai W. DNA excision repair at telomeres. DNA Repair (Amst). 2015; 3510.1016/j.dnarep.2015.1009.1017
18. Ambrus A, Chen D, Dai J, Bialis T, Jones RA, Yang D. Human telomeric sequence forms a hybrid-type intramolecular G-quadruplex structure with mixed parallel/antiparallel strands in potassium solution. Nucleic Acids Res. 2006; 34:2723–2735. [PubMed: 16714449]
19. Phan AT, Kuryavyi V, Luu KN, Patel DJ. Structure of two intramolecular G-quadruplexes formed by natural human telomere sequences in $K^+$ solution. Nucleic Acids Res. 2007; 35:6517–6525. [PubMed: 17895279]
20. Miller MC, Buscaglia R, Chaires JB, Lane AN, Trent JO. Hydration is a major determinant of the G-quadruplex stability and conformation of the human telomere 3′ sequence of $d(AG_3(TTAG_3)_3)$. J Am Chem Soc. 2010; 132:17105–17107. [PubMed: 21087016]
21. Gray RD, Trent JO, Chaires JB. Folding and unfolding pathways of the human telomeric G-quadruplex. J Mol Biol. 2014; 426:1629–1650. [PubMed: 24487181]
22. Gray RD, Buscaglia R, Chaires JB. Populated Intermediates in the Thermal Unfolding of the Human Telomeric Quadruplex. J Am Chem Soc. 2012; 134:16834–16844. [PubMed: 22989179]
23. Mashimo T, Yagi H, Sannohe Y, Rajendran A, Sugiyama H. Folding Pathways of Human Telomeric Type-1 and Type-2 G-Quadruplex Structures. J Am Chem Soc. 2010; 132:14910–14918. [PubMed: 20882978]
24. Lech CJ, Cheow Lim JK, Wen Lim JM, Amrane S, Heddi B, Phan AT. Effects of site-specific guanine C8-modifications on an intramolecular DNA G-quadruplex. Biophys J. 2011; 101:1987–1998. [PubMed: 22004753]
25. Vorlícková M, Tomasko M, Sagi AJ, Bednarova K, Sagi J. 8-Oxoguanine in a quadruplex of the human telomere DNA sequence. FEBS J. 2011; 279:29–39. [PubMed: 22008383]
26. Szalai VA, Singer MJ, Thorp HH. Site-specific probing of oxidative reactivity and telomerase function using 7,8-dihydro-8-oxoguanine in telomeric DNA. J Am Chem Soc. 2002; 124:1625–1631. [PubMed: 11853436]
27. Stadlbauer P, Trantirek L, Cheatham TE 3rd, Koca J, Sponer J. Triplex intermediates in folding of human telomeric quadruplexes probed by microsecond-scale molecular dynamics simulations. Biochimie. 2014; 105:22–35. [PubMed: 25038568]
28. Aggrawal M, Joo H, Liu W, Tsai J, Xue L. 8-Oxo-7,8-dihydrodeoxyadenosine: the first example of a native DNA lesion that stabilizes human telomeric G-quadruplex DNA. Biochem Biophys Res Commun. 2012; 421:671–677. [PubMed: 22538366]

29. Virgilio A, Esposito V, Mayol L, Giancola C, Petraccone L, Galeone A. The oxidative damage to the human telomere: effects of 5-hydroxymethyl-2′-deoxyuridine on telomeric G-quadruplex structures. Org Biomol Chem. 2015; 13:7421–7429. [PubMed: 25997822]
30. An N, Fleming AM, Burrows CJ. Interactions of the human telomere sequence with the nanocavity of the alpha-hemolysin ion channel reveal structure-dependent electrical signatures for hybrid folds. J Am Chem Soc. 2013; 135:8562–8570. [PubMed: 23682802]
31. An N, Fleming AM, Middleton EG, Burrows CJ. Single-molecule investigation of G-quadruplex folds of the human telomere sequence in a protein nanocavity. Proc Natl Acad Sci U S A. 2014; 111:14325–14331. [PubMed: 25225404]
32. Wolna AH, Fleming AM, Burrows CJ. Single-molecule analysis of thymine dimer-containing G-quadruplexes formed from the human telomere sequence. Biochemistry. 2014; 53:7484–7493. [PubMed: 25407781]
33. Shim JW, Tan Q, Gu LQ. Single-molecule detection of folding and unfolding of the G-quadruplex aptamer in a nanopore nanocavity. Nucleic Acids Res. 2009; 37:972–982. [PubMed: 19112078]
34. Karsisiotis AI, Hessari NMa, Novellino E, Spada GP, Randazzo A, Webba da Silva M. Topological Characterization of Nucleic Acid G-Quadruplexes by UV Absorption and Circular Dichroism. Angew Chem, Int Ed. 2011; 50:10645–10648.
35. Vorlickova M, Chladkova J, Kejnovska I, Fialova M, Kypr J. Guanine tetraplex topology of human telomere DNA is governed by the number of (TTAGGG) repeats. Nucleic Acids Res. 2005; 33:5851–5860. [PubMed: 16221978]
36. An N, Fleming AM, White HS, Burrows CJ. Nanopore detection of 8-oxoguanine in the human telomere repeat sequence. ACS Nano. 2015; 9:4296–4307. [PubMed: 25768204]
37. Reiner JE, Balijepalli A, Robertson JW, Campbell J, Suehle J, Kasianowicz JJ. Disease detection and management via single nanopore-based sensors. Chem Rev. 2012; 112:6431–6451. [PubMed: 23157510]
38. Branton D, Deamer DW, Marziali A, Bayley H, Benner SA, Butler T, Ventra MD, Garaj S, Hibbs A, Huang X, Jovanovich SB, Krstic PS, Lindsay S, Ling XS, Mastrangelo CH, Meller A, Oliver JS, Pershin YV, Ramsey JM, Riehn R, Soni GV, Tabard-Cossa V, Wanunu M, Wiggin M, Schloss JA. The potential and challenges of nanopore sequencing. Nat Biotechnol. 2008; 26:1146–1153. [PubMed: 18846088]
39. Wanunu M. Nanopores: A journey towards DNA sequencing. Phys Life Rev. 2012; 9:125–158. [PubMed: 22658507]
40. Song L, Hobaugh M, Shustak C, Cheley S, Bayley H, Gouaux J. Structure of straphylococcal α-hemolysin, a heptameric transmembrane pore. Science. 1996; 274:1859–1866. [PubMed: 8943190]
41. Dhakal S, Cui Y, Koirala D, Ghimire C, Kushwaha S, Yu Z, Yangyuoru PM, Mao H. Structural and mechanical properties of individual human telomeric G-quadruplexes in molecularly crowded solutions. Nucleic Acids Res. 2013; 41:3915–3923. [PubMed: 23396442]
42. Xu Y, Noguchi Y, Sugiyama H. The new models of the human telomere d[AGGG(TTAGGG)$_3$] in $K^+$ solution. Bioorg Med Chem. 2006; 14:5584–5591. [PubMed: 16682210]
43. An N, Fleming AM, White HS, Burrows CJ. Crown ether-electrolyte interactions permit nanopore detection of individual DNA abasic sites in single molecules. Proc Natl Acad Sci U S A. 2012; 109:11504–11509. [PubMed: 22711805]
44. Zhou J, Liu M, Fleming AM, Burrows CJ, Wallace SS. Neil3 and NEIL1 DNA glycosylases remove oxidative damages from quadruplex DNA and exhibit preferences for lesions in the telomeric sequence context. J Biol Chem. 2013; 288:27263–27272. [PubMed: 23926102]
45. Petraccone L, Trent JO, Chaires JB. The tail of the telomere. J Am Chem Soc. 2008; 130:16530–16532. [PubMed: 19049455]
46. Petraccone L, Spink C, Trent JO, Garbett NC, Mekmaysy CS, Giancola C, Chaires JB. Structure and stability of higher-order human telomeric quadruplexes. J Am Chem Soc. 2011; 133:20951–20961. [PubMed: 22082001]
47. Abraham Punnoose J, Cui Y, Koirala D, Yangyuoru PM, Ghimire C, Shrestha P, Mao H. Interaction of G-quadruplexes in the full-length 3′ human telomeric overhang. J Am Chem Soc. 2014; 136:18062–18069. [PubMed: 25438191]

48. Wang H, Nora GJ, Ghodke H, Opresko PL. Single molecule studies of physiologically relevant telomeric tails reveal POT1 mechanism for promoting G-quadruplex unfolding. J Biol Chem. 2010; 286:7479–7489. [PubMed: 21183684]

49. Xu Y, Ishizuka T, Kurabayashi K, Komiyama M. Consecutive formation of G-quadruplexes in human telomeric-overhang DNA: A protective capping structure for telomere ends. Angew Chem Int Ed Engl. 2009; 48:7833–7836. [PubMed: 19757477]

50. Ghosh A, Rossi ML, Aulds J, Croteau D, Bohr VA. Telomeric D-loops containing 8-oxo-2′-deoxyguanosine are preferred substrates for Werner and Bloom Syndrome helicases and are bound by POT1. J Biol Chem. 2009; 284:31074–31084. [PubMed: 19734539]

51. Fleming AM, Zhou J, Wallace SS, Burrows CJ. A role for the fifth G-track in G-quadruplex forming oncogene promoter sequences during oxidative stress: Do these “spare tires” have an evolved function? ACS Cent Sci. 2015; 1:226–233. [PubMed: 26405692]

52. Rhodes D, Lipps HJ. G-quadruplexes and their regulatory roles in biology. Nucleic Acids Res. 201510.1093/nar/gkv1862

53. Zhang B, Galusha J, Shiozawa P, Wang G, Bergren A, Jones R, White R, Ervin E, Cauley C, White H. Bench-top method for fabricating glass-sealed nanodisk electrodes, glass nanpore electrodes, and glass nanopore membranes of controlled size. Anal Chem. 2007; 79:4778–4787. [PubMed: 17550232]

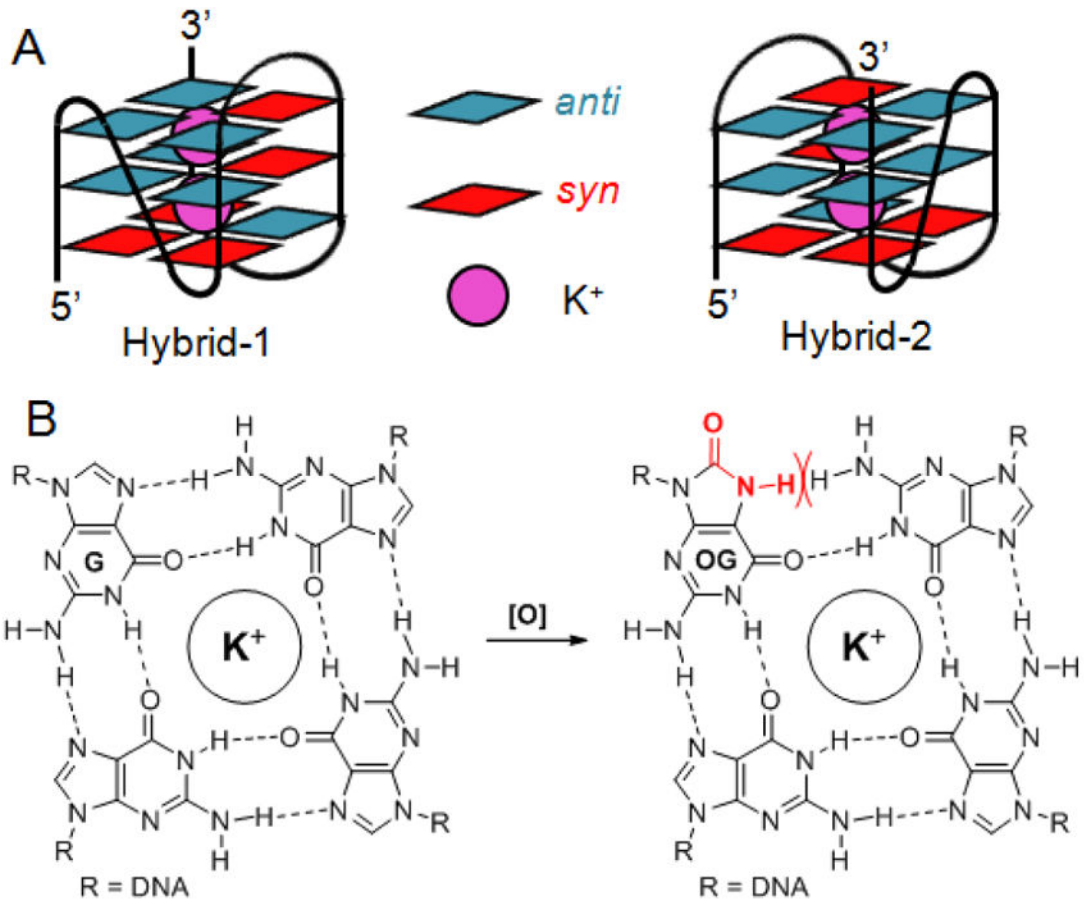


**Figure 1.**

Hybrid G4 folds of the human telomere sequence and scheme for oxidation of G to OG in a G tetrad. (A) Hybrid topologies observed for the human telomere sequence based on pdb 2JSQ and 2JSK.[19] (B) The H-bonding properties of G tetrads with and without OG.

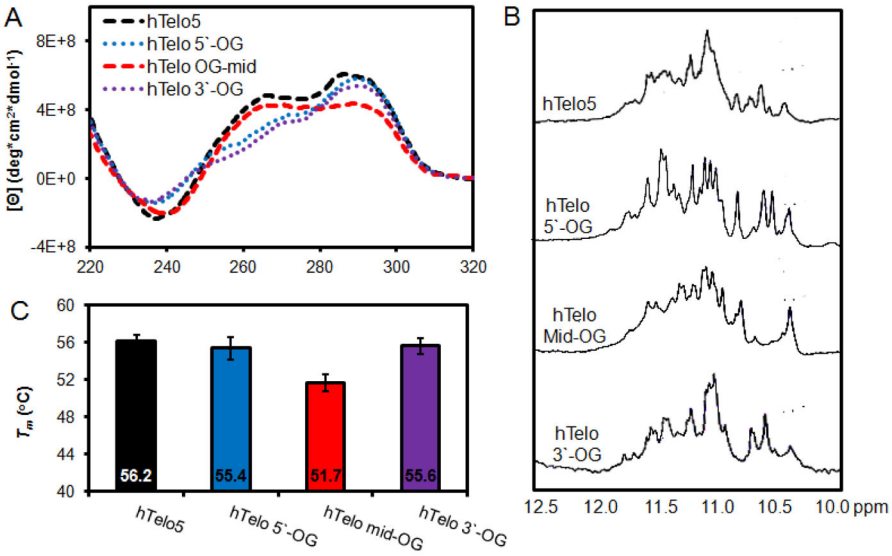


**Figure 2.**

Analysis of five-repeat hTelo sequences by CD, $^{1}$H-NMR, and $T_m$. The CD and $T_m$ studies were conducted in 140 mM KCl, 12 mM NaCl, 20 mM cacodylate buffer at pH 7.4 on samples with concentrations of 3 μM. The $^{1}$H-NMR spectra were recorded in 70 mM KCl 20 mM $KP_i$ buffer at pH 7.0 at 24 °C on samples with concentrations of 300 μM.

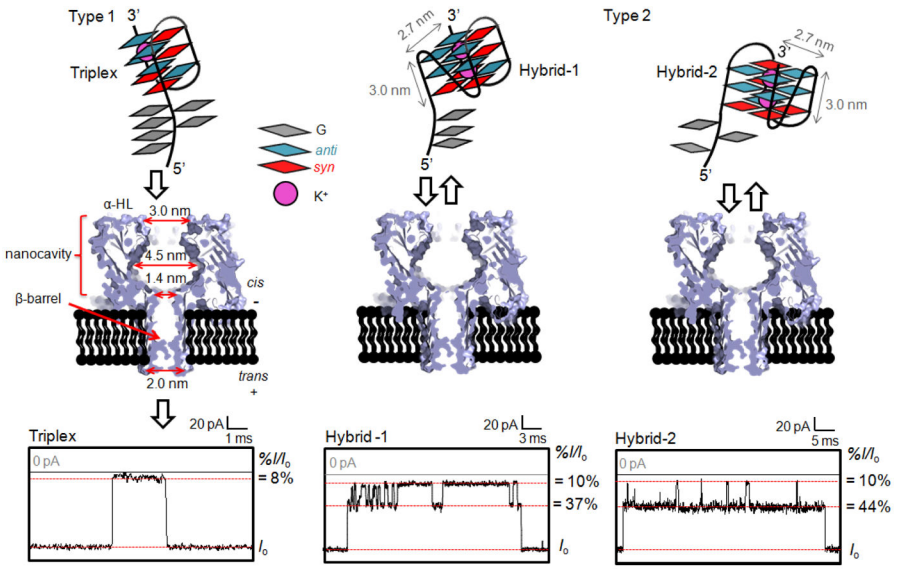


**Figure 3.**

Characteristic *i-t* signatures for triplex, hybrid-1, and hybrid-2 folds from the five-repeat human telomere sequence. The data were recorded on 5 μM G4 samples in 50 mM KCl, 950 mM LiCl, and 20 mM Tris pH 7.9 at 20 °C with a 120 mV (*trans* vs. *cis*) bias. The data were collected with a 100-kHz low-pass filter, and the *i-t* traces were refiltered to 20 kHz for presentation purposes. The dimensions for the hybrid G4s were derived from pdb 2JSQ and 2JSK,[19] while those for α-HL came from pdb 7AHL.[40]

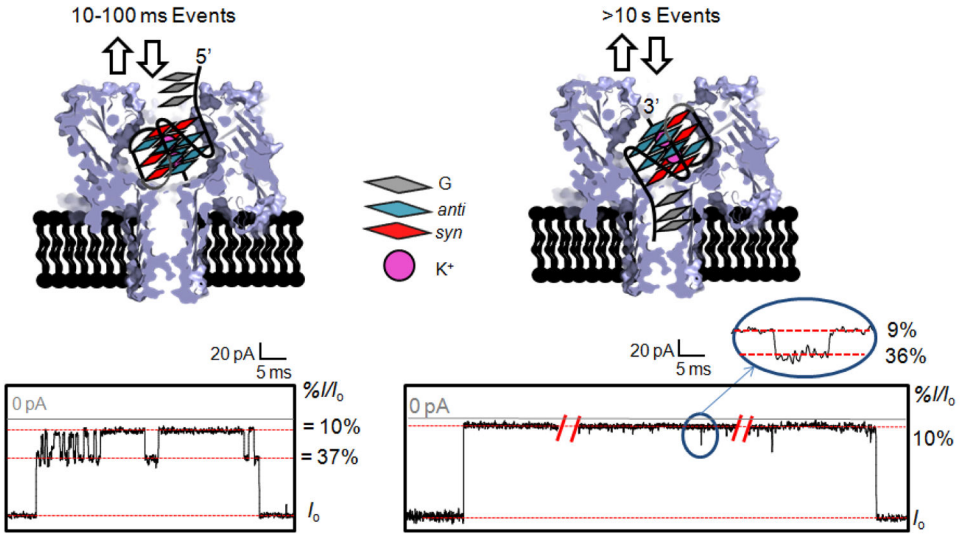


**Figure 4.**

Orientation-specific entry modes leading to two different unzipping times for the Type 2 events. The *i-t* trace lasting ~10 sec intentionally had sections of time removed for presentational purposes that is shown with the red bars; see Figure S3 for the entire *i-t* trace.

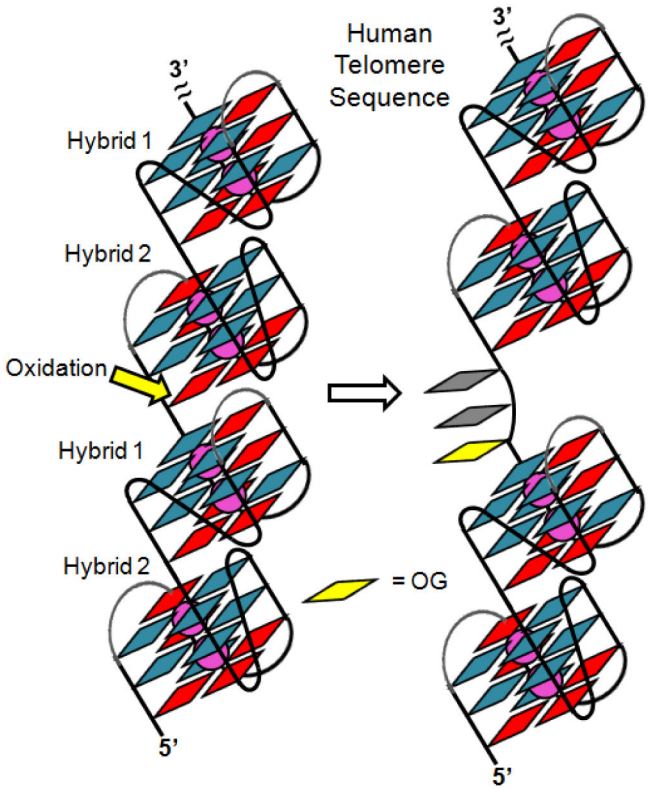


**Figure 5.**
Oxidation of G to OG in the human telomere causes looping out of the damaged G-track to maintain the folded structure.

**Table 1**

Five-repeat hTelo sequences studied.

| Name | Sequence* |
|---|---|
| hTelo5 | 5′-TA GGG TTA GGG TTA GGG TTA GGG TTA GGG TT-3′ |
| hTelo 5′-OG | 5`-TAXGG TTA GGG TTA GGG TTA GGG TTA GGG TT-3` |
| hTelo mid-OG | 5`-TA GGG TTA GGG TTA XGG TTA GGG TTA GGG TT-3` |
| hTelo 3′-OG | 5`-TA GGG TTA GGG TTA GGG TTA GGG TTA XGG TT-3` |

*X = 8-oxo-7,8-dihydro-2′-deoxyguanosine

**Table 2**

Distribution of triplex, hybrid-1, and hybrid-2 folds for the five-repeat telomere sequences studied with and without OG. The distributions were obtained from the characteristic *i-t* patterns recorded in the α-HL nanopore. The values were obtained from populations of >500 events and the errors are the standard deviations of three independent trials. n.d. = not determined

| | Type 1 | Type 2 | | |
|---|---|---|---|---|
| **Sequence** | **Triplex** | **Hybrid-1** | **Hybrid-2** | **Hybrid-1 : Hybrid-2** |
| hTelo5 | 21 ± 2% | 44 ± 5% | 28 ± 3% | 1.6 : 1.0 |
| hTelo 5′-OG | 24 ± 3% | 33 ± 3% | 36 ± 4% | 0.9 : 1.0 |
| hTelo mid-OG | 100% | n.d. | n.d. | n.d. |
| hTelo 3′-OG | 18 ± 2% | 45 ± 5% | 29 ± 3% | 1.5 : 1.0 |